ORNL/TM-2022/2566

Pulse-Strengthened and Laser Edge–Sealed Vacuum Insulation Glazing

Team: Pooran Joshi[1], Mahabir Bhandari[1], Sarma Gorti[1], Adrian Sabau[1], Derek Byrd[1], Thomas Muth[1], Ahmed Hassen[1], Lingyue Zhang[2], Wenyuan Zhu[2], Seungha Shin[2], Anming Hu[2], Bipin Shah[3]

[1]*Oak Ridge National Laboratory*
[2]*University of Tennessee, Knoxville*
[3]*WinBuild, Inc.*

Abstract

Scalable, low-cost processing strategy for glass strengthening and sealing is proposed to improve the thermal performance of insulating glass units and develop innovative window technologies. In this project, a combination of large-area photonic processing, additive manufacturing, and laser encapsulation techniques is reported to realize a vacuum glazing technology to meet the cost, performance, reliability, and throughput demands. A modeling framework for evaluating the mechanical and thermal response was established to verify the structural deformation and thermal conductance. Micro-size glass frits in printing ink and a continuous-wave laser curing were employed to allow the formation of a hermetic bonding layer and led to improvement of glass edge sealing. Various sealing parameters, including laser traveling speed, spot diameter, and laser power were optimized. The water seepage and mechanical strength of the resulting glass-to-glass bonding were examined as well. These results showcase the development of a practical vacuum insulating glazing with several unique features through a combination of photonic processing, laser encapsulation, and additive manufacturing.

Introduction

Maximizing the energy efficiency of the glazing used in buildings is of great importance since windows play a significant role in the building environment: they cover only 10–15% of wall area but account for 40% of the heat loss [1, 2]. To improve thermal insulation, glazing consists of two or more sheets of glass separated by an insulating space, which minimizes conductive and convective heat transfer. Further reduction of the radiative heat flow is achieved through transparent low-emittance coatings, which are generally applied on the internal surfaces of glass panes [3]. Among different glazing technologies, vacuum insulated glazing (VIG) is considered

OAK RIDGE National Laboratory

Oak Ridge National Laboratory is managed by UT-Battelle LLC for the US Department of Energy

U.S. DEPARTMENT OF ENERGY | Office of Science

to be a promising technology because of its lower thickness, higher thermal resistance, and effective soundproof performance, compared with conventional glazing [4].

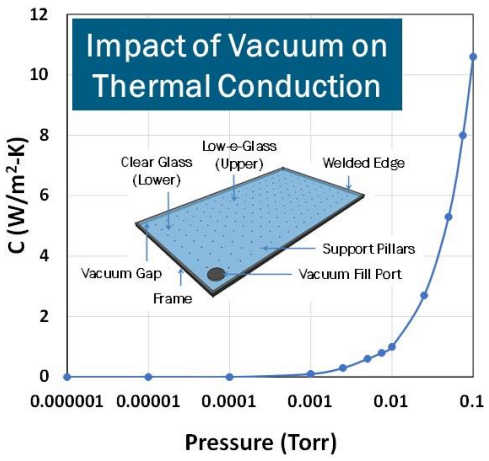

Figure 1 *Impact of vacuum on thermal performance of insulating glass units.*

One of the major challenges in vacuum glazing is the design of the seal between the two panes of glass for maintaining the vacuum and energy efficiency of the unit [5]. Since the thermal insulation performance is significantly dependent on the vacuum level (Figure **1**), overcoming the challenge in the seal design is critical to successful VIG development. In most cases, the glass-seal bonding is achieved by a thermo-compressive process in which the sealing is usually cured inside a furnace. However, furnace sealing requires the whole device to be heated, which can limit the use of multistep manufacturing processing and temperature-sensitive processes/materials inside the VIG unit, can lead to potential for off-gassing, and can reduce the heat efficiency and increase the complexity of the manufacturing process. To cope with this issue, more localized curing techniques have been developed. The laser-strengthening glass frit bonding technique, which combines the glass frit bonding and laser joining techniques, has been proposed, and it allows localized heating of the sealing material, thus protecting any temperature-sensitive materials located inside the devices [6]. Compared with the furnace sealing method, the laser-strengthening glass frit bonding technique is more cost-effective as the heat input is focused only on the sealing area instead of the whole glazing unit, thus resulting in reduced power consumption and increased heat efficiency. Moreover, the localized curing with laser enables a much faster and easier sealing process.

Another key point for the VIG unit is enhancing the effective thermal insulation. This requires optimizing the design of the gap between the glass panes, consisting of support pillars and vacuum, since it provides a thermal transport bottleneck for the overall heat transfer. Exploring all the possible VIG design parameters and comprehensively examining their effects through experiments is expensive and technologically challenging. Thus, computational simulations have been employed as a more economical and effective way to study the VIG thermal performance. Among simulation approaches, the finite element method (FEM) has been widely used for thermal and structural analysis of VIG because of its accuracy and efficiency in solving initial and boundary value problems for complex geometries [7]. In addition, using the 3D FEM simulations, the effects of various pillar design parameters, such as pillar shape, contact area, height, and arrangement, can be comprehensively evaluated for an optimized VIG design.

In this project, a cost-effective laser encapsulation technique combined with additive manufacturing, plasma glass strengthening, and photonic processing for the VIG unit is reported. The modeling framework for the mechanical and thermal response evaluation was established to verify the structural deformation and thermal conductance of the VIG. Design of low thermal conductivity pillar spacers, secondary edge seal, and vacuum valve were also included to realize an integrated VIG technology.

R&D Focus

This project focused on a scalable, low-cost processing strategy for glass strengthening and sealing to improve the thermal performance of insulating glass units. A combination of large-area photonic processing, additive manufacturing, and laser encapsulation techniques was pursued to realize a vacuum glazing technology to meet the cost, performance, reliability, and throughput demands. The specific aims of the proposed research and development (R&D) to realize an integrated VIG technology included scalable pulse thermal processing for in-line glass strengthening, laser-assisted hermetic sealing, and additive manufacturing of low thermal conductivity pillar spacers, secondary edge seal, and vacuum valve. The integration of materials, component design, and manufacturing innovation attempts to address the technology adoption considerations of an insulated glass manufacturer or an end window manufacturer.

Modeling for Structural and Thermal Characteristics

The effects of various pillar design parameters on the thermal insulation and mechanical performance of the VIG were investigated using finite element analysis (FEA) simulation software ABAQUS [8]. Figure 2 describes the model configuration for thermal and structural analysis. The results for the thermal conductance computed using the FEA model were verified against experimental data and analytical calculations. We also investigated the effects of edge-sealing design on the thermal and mechanical performance of VIG using FEA simulation software and experimental measurements.

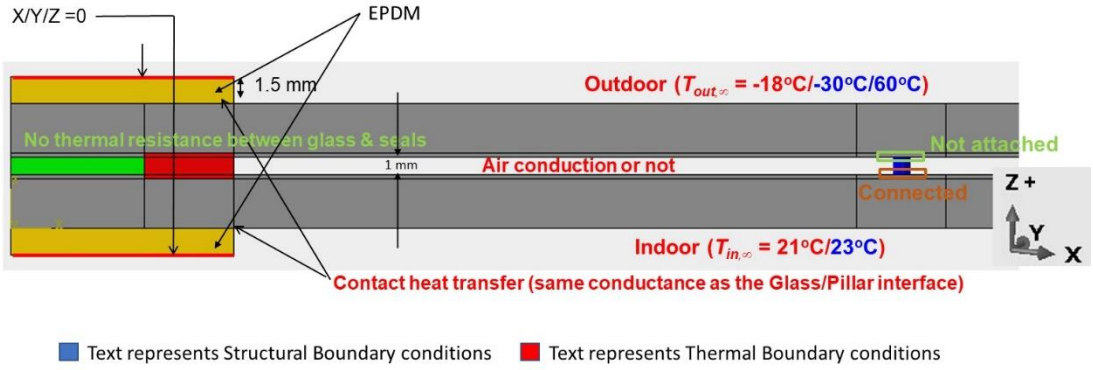

***Figure** 2 Modeling specification for thermal and structural analysis.*

Structural Deformation

As vacuum is introduced within a VIG window, the pressure difference between the vacuum and atmospheric pressure deforms the glass panes. Under severe glass deformation, the two glass panes can be in contact, creating a new conduction path, which brings a sharp increase in the *U*-value (overall heat transfer coefficient). To prevent the glass from collapsing under vacuum pressure, very small pillars are placed at regular intervals between the glass panes. These pillars also provide structural support under different stresses caused in the cavity by service conditions. To confirm that the modeled VIG was not significantly distorted because of the pressure difference, structural analyses (using FEA simulations) were conducted with the quarter-window VIG model by taking advantage of the symmetry in the VIG unit to limit the size of the computational domain. Symmetry boundary conditions were applied to the two sides of the model that

correspond to the centerline along the *x* and *y* directions of the full VIG, and the nodes along the top and bottom surface of the EPDM (ethylene propylene diene monomer) frame were constrained to have zero displacement (Figure 2). Frictionless contact was assumed between each pillar and the top glass pane, and a cohesive interface with a stiffness of 10^3 N/mm^3 was assumed between each pillar and the bottom glass pane. A pressure load of 1 atm was directly applied to the outside surfaces of both glass panes, and the pressure in the gap between the glass panes was set to 0.133 N/m^2 (10^{-3} Torr). Heat transfer coefficients on the outer surfaces of the outdoor (C_{out}) and indoor (C_{in}) glass panes were set to 29.41 and 6.67 W/m^2-K, respectively. These boundary conditions were taken in accordance with ASTM C1199 testing procedure. The emissivity of the glass surface was assumed to be 0.84, except for the inner surface of the top glass, which was set to 0.018 because of a low-emissivity coating. Assuming extreme weather conditions, 60°C and −30°C were used for the outdoor temperatures (T_{out}), and the indoor temperature (T_{in}) was fixed at 23°C to simulate ASTM E2188 and E2190 durability test conditions. Using thermo-mechanical simulations with a quarter-window model, the displacement in the z direction (i.e., perpendicular to glass surface) was calculated as presented in Figure 3a–3d. The stress distribution was evaluated along a path across the two glass panes and a pillar in the center area for the case with $T_{out} > T_{in}$, as shown in Figure 3e.

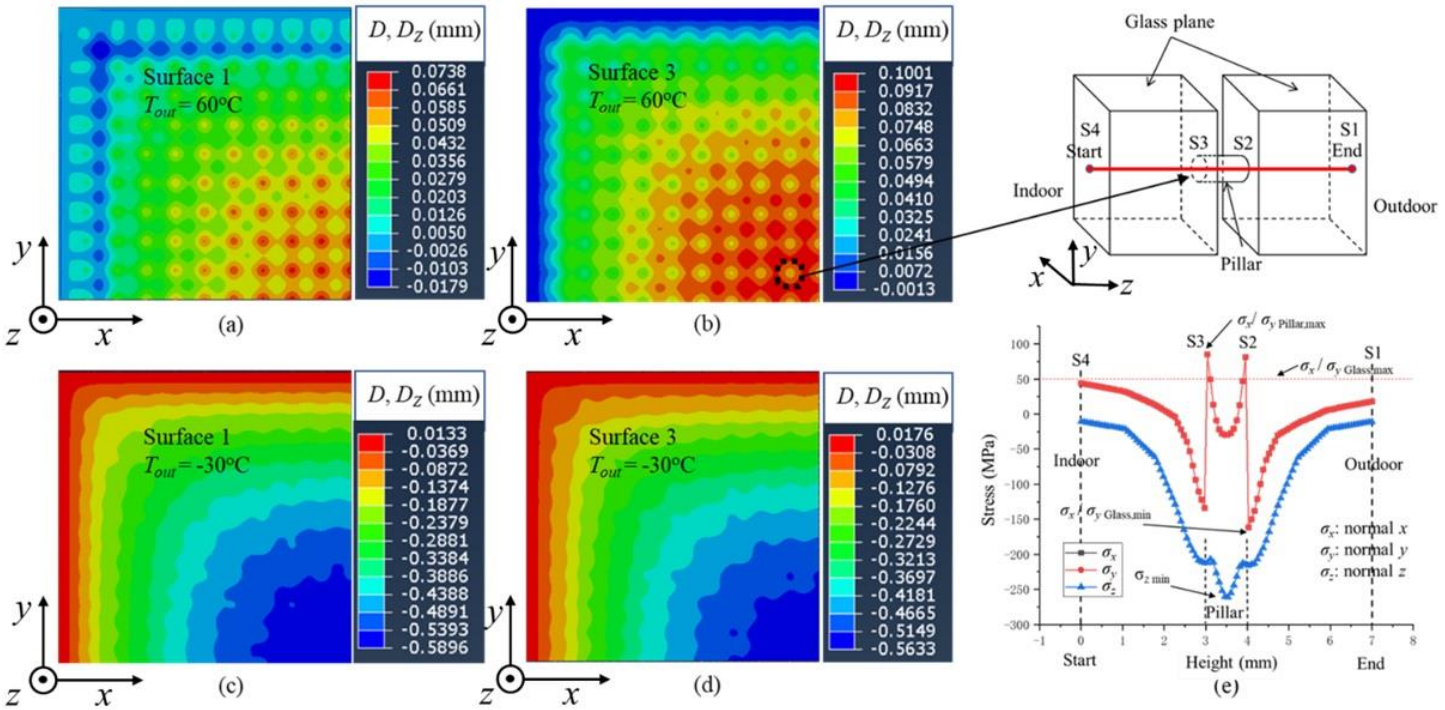

Figure 3 *(a–d) Glass displacement in the z direction with the surface selection for T_{out} = 60°C and T_{in} = 23°C: displacement (a) on the exterior surface of the outdoor glass (S1) and (b) on the inner surface of the indoor glass (S3). For a cold outside (T_{out} = −30°C): displacement (c) on the exterior surface of the outdoor glass (S1) and (d) on the inner surface of the indoor glass (S3). (e) Stress distribution along a path through the indoor glass, a pillar in the center region, and outdoor glass as shown in the schematic.*

Thermal Effect of Pillar Parameters

Based on the analysis of the FEA results, lower pillar thermal conductivity (k_{pa}) and higher pillar height (h) directly reduce the heat loss, especially when k_{pa} is lower than 50 W/m-K (Figure 4a). If VIG contains pillars with k_{pa} higher than 50 W/m-K, the effects of pillar thermal conductivity and pillar height become minor. In addition to cylindrical pillars, other pillar geometrical shapes were examined. Figure 4b presents the thermal performance of rectangular parallelepiped pillars. The U-value increased with aspect ratio l_1/l_2 for the rectangular pillars, suggesting a smaller aspect ratio (or smaller perimeter) for thermal insulation (i.e., square shape) has the lowest U. The aspect ratio dependence of the U-value was more significant for a higher k_{pa}, and similarly, a larger aspect ratio led to a larger k_{pa} dependence (especially at lower values of k_{pa}).

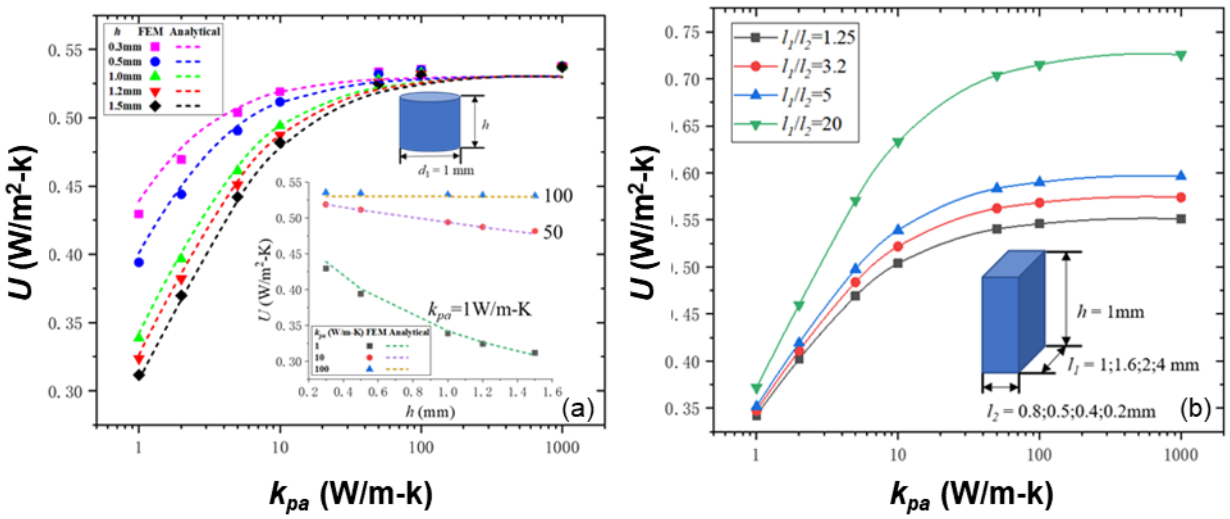

Figure 4 *(a) U-value with respect to k_{pa} with different heights of cylindrical pillar (h = 0.3, 0.5, 1.0, 1.2, and 1.5 mm) and (b) with different aspect ratios (l_1/l_2 = 1.25, 3.2, 5, and 20) of rectangular parallelepiped pillar with a fixed contact area (A = $l_1 l_2$ = 0.8 mm^2).*

In other geometry designs, the horizontal cylindrical pillar arrangement has been shown to enhance thermal performance, resulting in more than 25% reduction in U-value compared with the vertical cylinder (Figure 5a). Smaller pillar volume and smaller contact area (between pillar and glass pane) with a smaller perimeter leads to better thermal performance to VIG. However, the influence of the contact area is more significant than that of the pillar volume, and even under the same value of contact area, different perimeters will significantly affect the overall U-value. An expression for thermal conductance applicable to a rectangular parallelepiped pillar array was developed to help better describe the thermal performance of VIG with noncylindrical pillars (Figure 4b). Increase in the pillar spacing (λ) leads to a decrease in the U-value; however, this influence becomes less significant when the pillar spacing becomes larger than 50 mm (Figure 4a). The main reason is the reduction in the number of pillars in the VIG, which leads to a decrease in the gap thermal conductance, and hence, the overall U-value. In addition, the effect of the pillar height becomes less significant with larger pillar spacing (Figure 5b). Based on various pillar design considerations, we conclude that each pillar parameter has a significant effect on the thermal performance of VIG, and some of the parameters, such as pillar volume, pillar contact area, and pillar body shape, need to be considered together when enhancing the thermal performance of VIG (Figure 5). Current analytical formulas for U-value are limited to consideration of cylindrical pillars and need to be improved to account for other pillar shapes and arrangements. In addition, the analytical expressions were derived without consideration of the edge effects, which include the primary and secondary seals and the frame. Including the edge effects can cause a significant increase in the U-value

compared with the idealized unit cell; therefore, analytical expressions must be used with caution when applied to the design of VIG. VIG can be optimized for better thermal performance through the thermo-mechanical analyses based on FEM simulations as described in this report.

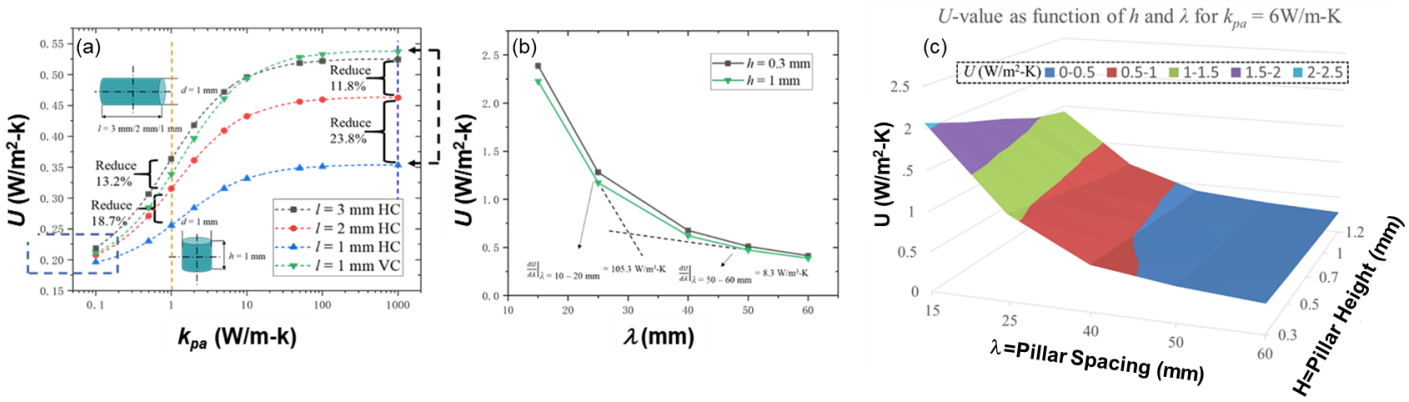

Figure 5 (a) Variation of U-value for horizontal cylindrical pillars and vertical cylindrical pillars with respect to the pillar thermal conductivity (k_{pa}). (b) Two-dimensional plot of U-value for different pillar heights and spacings with k_{pa} = 6 W/m-K; dU/dλ is the slope value of the U-value with respect to pillar spacing. (c) Three-dimensional plot of U-value for different pillar heights and spacings with k_{pa} = 6 W/m-K.

Effects of Sealing Design

To study the seal thermal effect in greater detail, the heat flux distribution from the edge to the center of the VIG was examined. We chose two different paths close to one of the symmetry planes of the VIG FEA model. While path 1 at the symmetry plane on the top surface of the outdoor glass pane goes through the *xy* locations of the center of the support pillars, path 2 is shifted by a distance of *λ/2* relative to path 1 so that it does not go through any of the support pillars. A schematic illustration of the two paths is shown in Figure 6a, and the results of heat flux distribution are presented in Figure 6b and 6c.

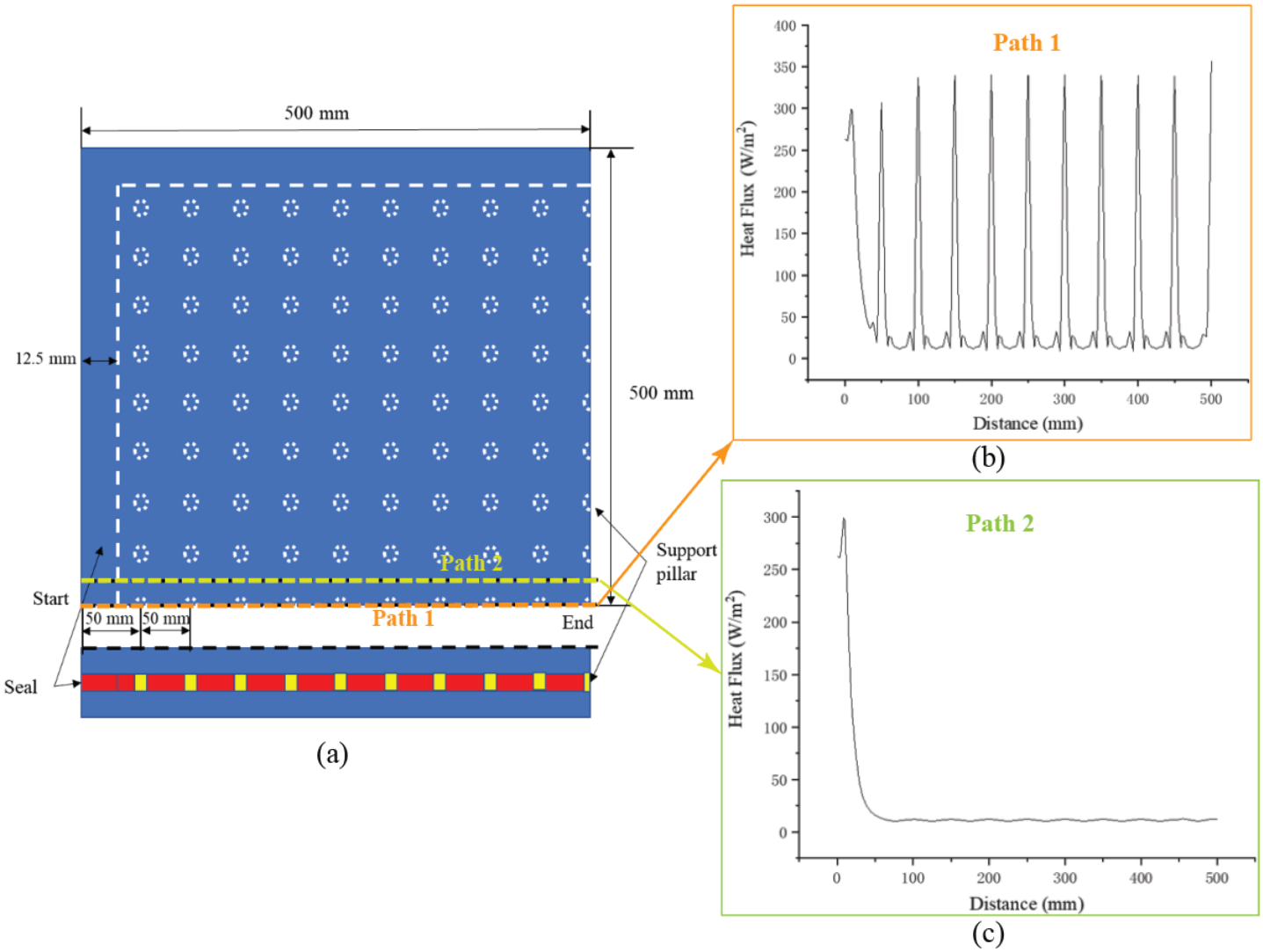

Figure 6 *(a) Schematic of VIG FEA model showing two different paths, with path 1 along the center of the VIG and path 2 shifted by 25 mm (λ/2) from path 1. (b) Heat flux distribution along path 1 and (c) along path 2 with* k_{seal} *= 1 W/m-K and* k_{pa} *= 16 W/m-K.*

Based on the results, it is observed that the heat flux variations along the two paths show considerable differences. Along path 1, which includes the effect of the pillars, there are local peaks in the heat flux at the locations corresponding to each pillar, whereas the heat flux distribution along path 2 shows minimal effect due to the pillars. After the initial decrease in the heat flux past the edge region, the heat flux distribution becomes more dependent on the pillar properties, and beyond about 100 mm, the effect of the edge section becomes negligible. Therefore, to better understand how the thermal conductivity values of the seal (k_{seal}) and of the pillar (k_{pa}) affect the heat flux distribution, we chose a 0–100 mm section of path 1 and path 2 as the new test range to study the influence of different values of k_{pa} and k_{seal}.

We calculated the heat flux distribution for different values of the pillar thermal conductivity k_{pa} 1–999 W/m-K) along a portion of path 1 (0–100 mm) and path 2 (0–100 mm), with the thermal conductivity of the seal kept fixed at k_{seal} = 1 W/m-K. From the plots in Figure 7and 7b, the heat flux around the seal has a high

value and generally decreases beyond 12.5 mm, which represents the extent of the seal. The pillar thermal conductivity has an effect on the distribution of the heat flux along path 1 when the distance is larger than about 35 mm, which is almost three times longer than the width of the seal. The local peaks in the heat flux at the pillar locations increase with k_{pa}, although this increase becomes much smaller for k_{pa} larger than 16 W/m-K. Along path 2, the pillar thermal conductivity effect is also observed beyond about 35 mm, although the differences are very minimal for different k_{pa} values.

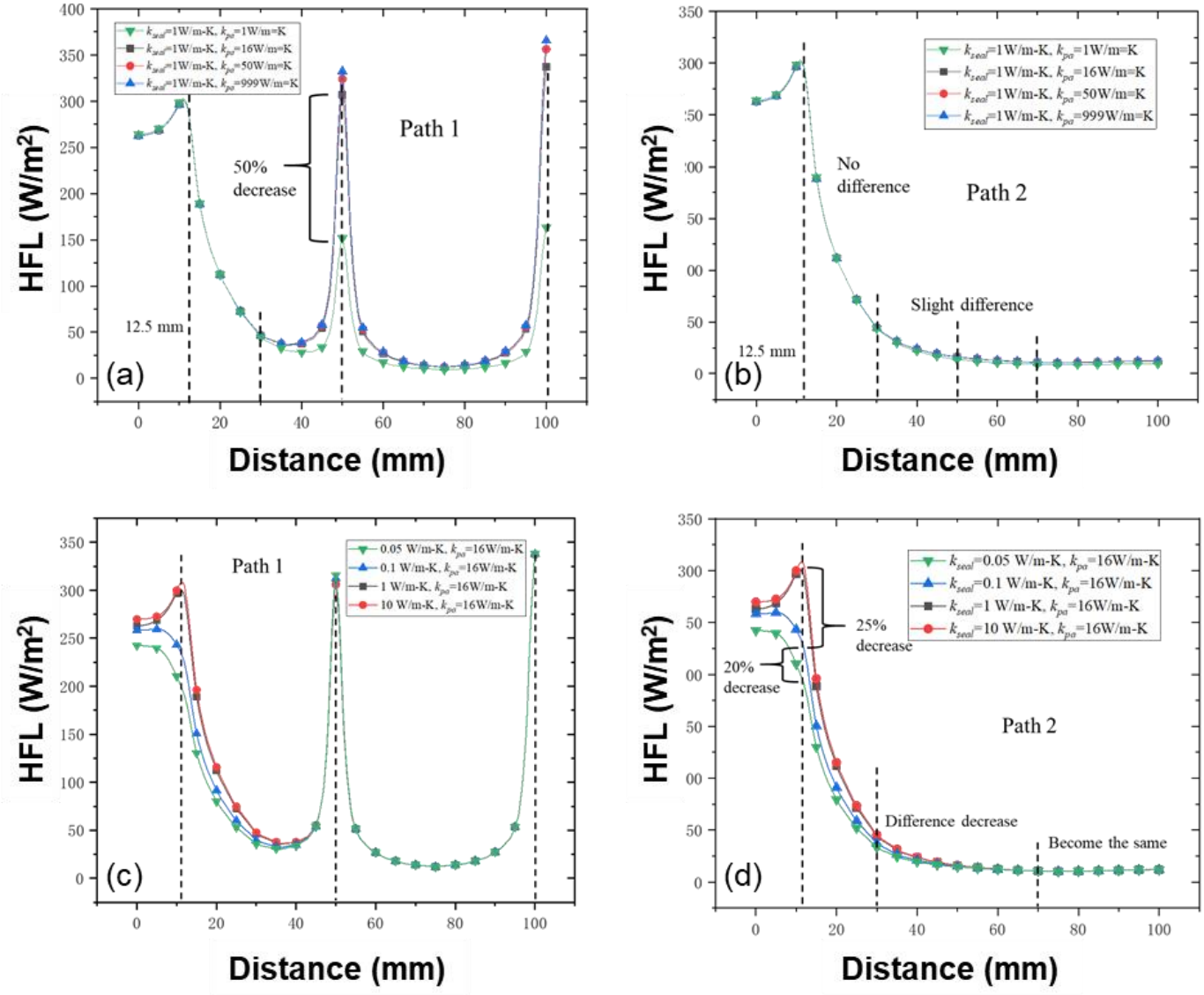

Figure 7 *Heat flux distribution along two different paths for different k_{seal} and k_{pa}: (a) heat flux distribution along path 1 with k_{seal} =1 W/m-K and k_{pa} = 1-999 W/m-K; (b) heat flux distribution along path 2 with k_{seal} =1 W/m-K and k_{pa} = 1–999 W/m-K; (c) heat flux distribution along path 1 with k_{seal} =0.05–10 W/m-K and k_{pa} = 16 W/m-K; and (d) heat flux distribution along path 2 with k_{seal} =0.05–10 W/m-K and k_{pa} = 16 W/m-K.*

Figure 7c and 7d show the heat flux distribution for different seal conductivity values k_{seal} (0.05–10 W/m-K), while the pillar conductivity is fixed at k_{pa} = 16 W/m-K. The thermal conductivity of the seal does not have a significant influence beyond about 35 mm, as noted previously. Along path 2, when the distance is larger than

35 mm, the heat fluxes for different k_{seal} values show only a slight difference, and this difference disappears beyond 70 mm. For both paths, the maximum heat flux difference is at the edge of the seal, which shows a 25% decrease when k_{seal} is reduced from 1 W/m-K to 0.1 W/m-K and a 20% decrease when k_{seal} is reduced from 0.1 W/m-K to 0.05 W/m-K.

Experimental Measurement of Mechanical Strength and Sealing Tightness

A flexible sealant mix containing a proprietary mix of ceramics and fluoropolymers was prepared. This paste was then enhanced with the addition of nano-size glass powder. As the fraction of glass powder increases, the flexible seal mix loses its fluidity before curing. With the ratio larger than 40%, the seal mix does not have sufficient fluidity to make an adequate seal; therefore, the flexible seal mix with glass powder fractions below 40% (0%, 10%, 20%, and 30%) was tested to investigate the shear strength and airtightness. All the tested samples (38 x 76 mm) of flexible seal with 10–30% ratio of glass power mixed presented no water leakage or any water vapor after 48 hours of sinking in water, demonstrating an effective sealing performance. No water leakage was observed in the sealing of 6 × 6 in. glass panes either, indicating that a larger size of glass panes can also achieve an airtight seal. The shear strength test showed that increasing the ratio of glass powder in the flexible seal mix results in lower maximum shear stress. When the ratio of mixed glass powder increased from 0% to 30%, the maximum shear stress τ_{max} decreased by 1.1%; however, when the ratio of glass powder increased from 30% to 35%, the τ_{max} decreased by 16.5%. That is, at up to 30%, the fraction of glass powder does not have a significant effect on the mechanical strength of the seal, while a content larger than 30% deteriorates the strength (Figure 8a–8c).

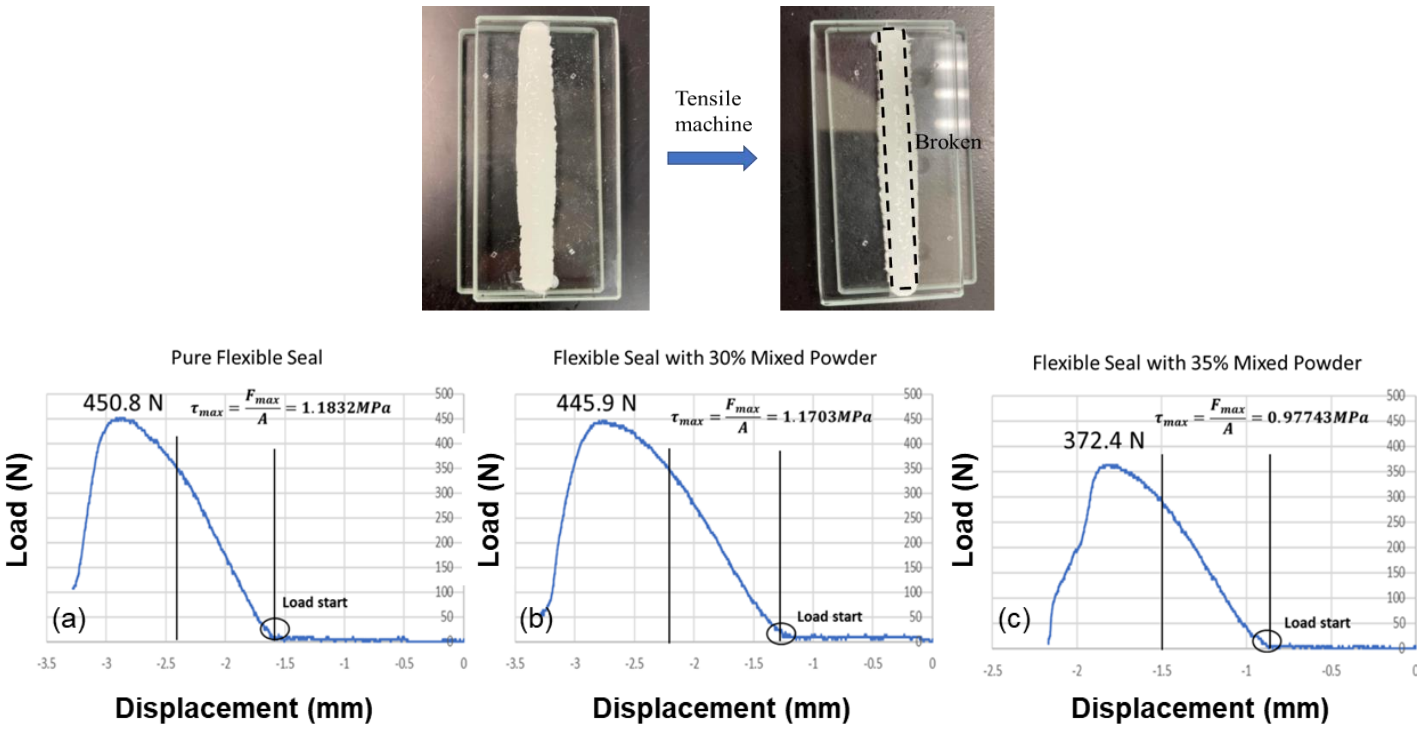

Figure 8 *Shear stress test using a tensile testing machine and a sample of glass with a flexible seal. Shear stress test results for glass with three different seals: (a) pure flexible seal, (b) flexible seal mixed with 30% glass powder, and (c) flexible seal mixed with 35% glass powder.*

Based on the analysis of FEM results, it was found that lower seal conductivity k_{seal} leads to a lower *U*-value of the VIG system, although the extent of this influence depends on the range of k_{seal}; if k_{seal} > 1 W/m-K, the influence becomes less significant, with only a 5% difference in *U*-value from k_{seal} = 1 W/m-K to k_{seal} = 10 W/m-K. The heat flux distribution indicated that the region affected by the seal can extend to about three times the width of seal and that the seal conductivity k_{seal} could affect the value of the heat flux around the seal, especially when k_{seal} is smaller than 1 W/m-K. However, this influence becomes smaller and smaller when k_{seal} is larger than 1 W/m-K or when the distance from the seal is more than three times the width of the seal. We also employed the pillar conductivity k_{pa} as a changeable parameter, but it does not show any significant influence on the sealing effect.

The flexible seal with different ratios of fine glass powder was tested in our experiments. When the volume fraction of the glass powder in the flexible seal was below 30%, it performed very well during the test, with no water leakage. However, when the ratio was larger than 40%, the seal material would lose most of its fluidity and could not be used to adequately bond and seal the glass panes. In addition, the higher volume fractions of glass powder led to considerable deterioration of the shear strength. Comparisons with FEA simulation results showed that the measured shear strength value (i.e., the maximum stress that the material can withstand before failure) for the seal with <30% glass powder was around 1.2 MPa (see Figure 8), and this value was 2–10 times larger than the calculated shear stress values (which ranged from 0.09–0.42 MPa for a seal elastic modulus of 20–100 MPa, with a larger modulus leading to larger stress). The very low elastic modulus (3–4 MPa) of the flexible seal developed in this work provides confidence in its capability to withstand the thermal and mechanical loads and to maintain adequate vacuum conditions during service, even in a 1 × 1 m working VIG system.

Using the measured shear stress and strain, the shear moduli (*G*) of the flexible seal samples were evaluated for use in determining the elastic moduli using the formula [$E = 2G(1 + \nu)$], and the resulting elastic modulus (*E*) of our 30% mix was 3.78 MPa. This value is very low compared with the elastic moduli of edge seals used by current VIG manufacturers and researchers, which normally are in gigapascals. This makes our edge seal unique and flexible.

Glass Strengthening: Scalable Plasma-Arc Lamp Photonic Processing

The ubiquitous presence of surface flaws limits the strength of glass articles. The range of practical strengths for glass used in everyday applications can vary over six orders of magnitude, which is indicative of the extensive range of flaw sizes that might exist or can be introduced into glass. The development of a robust glass strengthening technique for both thin and thick glasses will address and redefine the critical cost, weight, thickness, and reliability requirements for diverse applications. The plasma-arc lamp (PAL) heat source offers a mass production scale and a relatively safe, environmentally friendly, and economically viable method for strengthening glass. The plasma, which has a temperature in excess of 10,000 K, is stable and produces a broadband radiant spectrum in the range of 0.2–1.4 µm. The present system at Oak Ridge National Laboratory incorporates a new reflector designed to attain a source heat flux of 11 MW/m^2. In addition, the new reflector has been fabricated with two ports for monitoring the specimen condition during plasma arc lamp processing/testing using pyrometers and an infrared (IR) camera and/or video camera. PAL processing investigation focused on a low thermal budget processing approach to impact glass strength. As highlighted in Figure 9, in the investigated process space, the scalable PAL processing technique has shown an effective

tuning of the glass compressive stress in the range of 3–38 MPa that overlaps the strength requirement window of float glass and heat-strengthened glass applications. The processing time for various samples was in the range of 2–14 seconds, indicating an opportunity for high throughput glass strengthening for current and emerging thin glass window technologies.

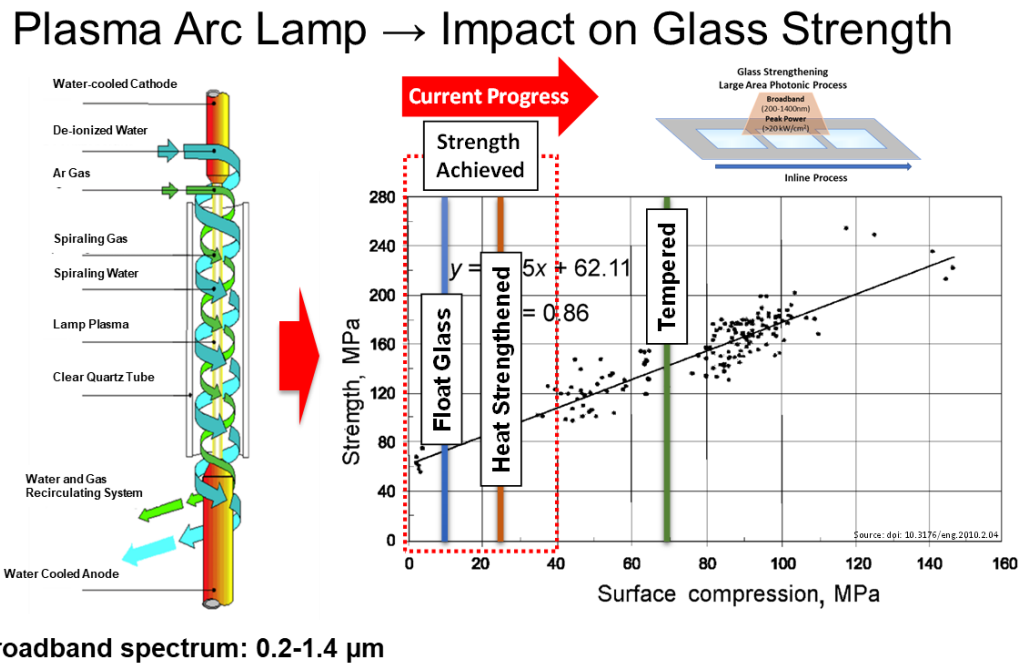

Figure 9 *Scalable photonic processing to impact thin glass strength for emerging window technologies.*

Digital Printing and Laser-Assisted Sealing for VIGs

Hermetic encapsulation to protect from the surrounding environment and maintain the internal environment is one of the most common requirements for several glass integrated device technologies such as organic light-emitting diodes and photovoltaic cells. The present investigation focused on digital printing of a glass frit paste onto the substrate and then using an IR laser beam to locally supply the necessary energy to allow the formation of a hermetic bonding layer. The glass frit bonding approach offers advantages of superior hermeticity, less stringent surface roughness requirements, and tailored expansion matching to the materials being joined. The laser glass frit sealing process is suitable for VIGs because of the high transparency of glass at the near IR laser wavelengths of interest. When the frit is exposed to a laser beam at a wavelength tailored for the frit absorption, the frit highly absorbs the laser light and converts the light into heat. Additionally, the laser-assisted glass frit bonding does not require the use of a glazing step and the application of pressure during the bonding step, which reduces the risk of misalignment of the

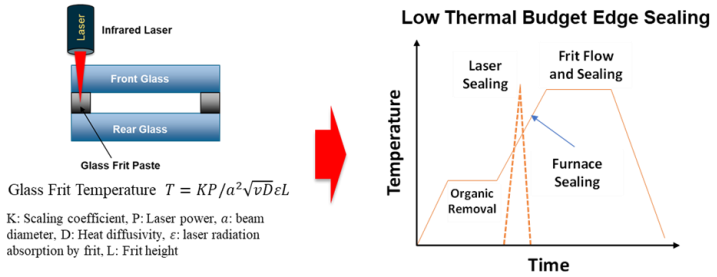

Figure 10 *Low thermal budget infrared laser process for edge seal*

substrates and lowers the thermal energy needed and sealing time of the overall process. The low temperature and low-thermal budget processing approach, as detailed in Figure 10, for encapsulation of vacuum insulation glasses aligns with the cost and throughput demands of the VIG manufacturing technology.

Emerging digital materials printing techniques offer significant cost advantages compared with conventional manufacturing techniques while addressing the time, space, and waste issues. Digital printing systems are capable of printing features from the nanometer to millimeter scale on both flat and conformal substrates. Inkjet printing is currently one of the lowest-cost direct write techniques that is moving from lab-scale to manufacturing scale. In the present work, a Voltera V-One printer was used to print the edge sealing layer using glass frit ink (Source: YEK Glass Co., Ltd, Model No. AMO-1411). The V-One printer can dispense any ink, paste, or viscous liquid with ±10 micron accuracy. The V-One heated bed allows for custom curing profiles up to 240°C. As highlighted in Figure 11, the direct-write printing technique allows for additive integration of materials using computer-aided design (CAD) files. For edge seal printing, the digital printing process was optimized to print the glass frit ink onto the glass substrate in a layer-by-layer manner with a thickness control from 50 to 250 µm for each layer. The printed samples were dried on the printer for 20 minutes at a platen temperature of 200°C. The platen temperature was increased at a ramp rate of 10°C/min to eliminate any thermal stress–induced cracks in the glass substrate.

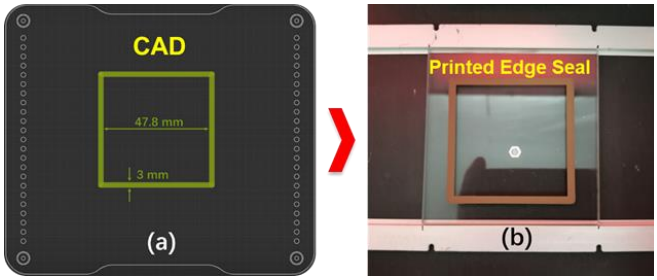

Figure 11 *Design to Printing employing digital*

Simulations were conducted with COMSOL Multiphysics software (COMSOL Inc., 2020) to identify the optimum IR (808nm) laser process window. In our experiment, laser power and *x-y* translation stage speed were the main process variables. Although a high temperature is required to realize glass frit melting and bonding, excessive heat coupling to the glass can result in cracks. A combination of laser power and translation speed dictates the heat coupling into the top/bottom glass and edge seal layer. Although both high laser power with high traveling speed and low power with low speed can lead to the same glass temperature, the spatial temperature distribution can be different due to different heat penetration lengths. In the simulations, the power of the heating source was adjusted to achieve a maximum temperature of 400°C. The bottom glass temperature was kept constant at 50°C. However, the heat coupling in the glass frit layer is dictated by the material absorption characteristics. The simulated isotherms showed a more efficient heat-flux transfer to the top glass pane at a translation speed of 1 mm/s compared to 5 mm/s. The temperature gradient increased across the glass pane with increasing feed rate, which led to a higher thermal stress. To eliminate the possibility of glass cracking, the laser process optimization focused on minimizing the laser power and the translation speed for optimum curing conditions. The laser process window was narrowed down to a translation speed range of 0.3–0.5 mm/s and a laser power range of 28–35 W for a 3 mm spot size to minimize the thermal stress and eliminate cracking issues. The laser scan velocity was limited to a value from 0.3 mm/s to 0.5 mm/s, and the laser power was limited from 28 to 35 W based on the experiment (at 35 W the glass cracks as soon as the laser starts). The simulated shear strength in this process range compared well with the experimental results. Figure 12 shows the measured shear stress of the sealed samples as a function of the laser power and the translation stage speed. The optimum process conditions appeared to be in the middle of the parameter domain, which matched well with the modeling predictions. Overall, it was

established that an increase of laser power during the sealing process should be followed by a higher translation speed to avoid thermal gradient–induced cracking issues.

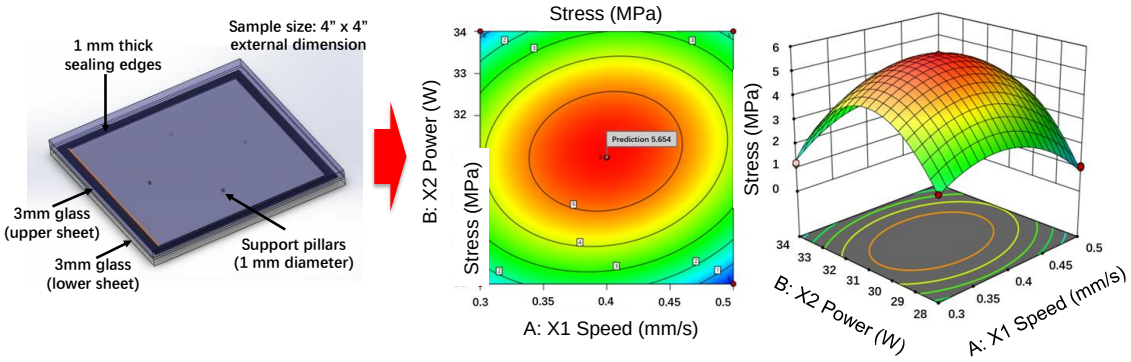

Figure 12 *COMSOL heat transfer analysis to optimize laser process for high throughput edge sealing.*

Printed Seal Performance

The performance of the laser-cured edge seal unit was evaluated in terms of the shear stress, hermetic sealing, and thermal characteristics. The shear stress test was conducted using the universal testing machine at a pushing speed of 5 mm/min and a maximum transduced load of 500 N. The maximum shear stress that the sample processed at a translation speed of 0.4 mm/s and a laser power of 31 W could withstand was measured to be 5.68 MPa, as shown in Figure 13, which was close to a value of 5.654 MPa predicted by the developed response surface methodology. Comparison of the shear stress of a thermally cured sample with the laser-processed sample showed the effectiveness of the laser processing in achieving a high strength at a significantly lower thermal budget to realize a practical technology.

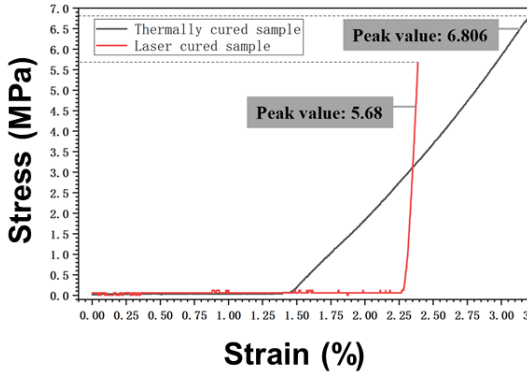

Figure 13 *Shear stress tests conducted on laser processed and thermally cured VIG*

The hermetic sealing characteristics of the laser-cured edge seal were established in terms of the water leakage characteristics in both the water inflow and outflow configurations. For outflow testing, a hole in the sealing line was created during the glass frit ink printing. After laser curing, the sample was filled with red-dyed water, and glass glue was applied to close the hole. To test leakage, the sample was immersed in a clean water bath. For water inflow testing, the laser processed sample was immersed in a red-dyed water bath to hold the gap part. In both configurations, no edge seal leakage was detected even after 48 hours of soaking. The observed results show promise for efficient curing of the edge seal layer at low thermal budgets, meeting the process scaling and high throughput requirements of a manufacturing platform.

The thermal performance of the thermally cured VIG unit was evaluated using a heat flux sensor with a sensitivity of 2.01 μV(W/m^2). The samples with the digitally printed edge seal layer were thermally annealed at a pressure of 1 mTorr. The gap between the top and bottom glass pieces was about 1 mm. The samples were placed on a hot plate maintained at a temperature of 70°C while the heat flux sensor was placed on the top glass as shown in Figure 14. The bare plates showed a size-dependent heat flow characteristic, while the VIG sample showed superior thermal performance compared with bare glass plates placed on the hot plate.

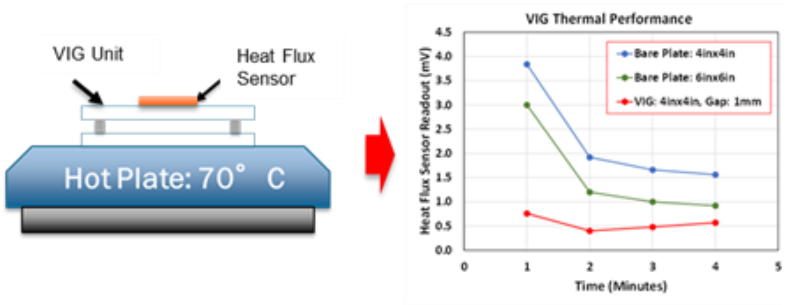

Figure 14 *Thermal performance of a VIG unit as evaluated using a heat flux sensor.*

Additive Manufacturing of VIG Components

The digital direct-write printing technique shows promise for scalable printing of the edge seal layer for VIG applications. The emerging ink-based materials printing techniques combined with the laser-processing approach offer an opportunity for direct integration into the manufacturing line. Aside from digital printing of the edge seal layer, the digital printing process was further explored for direct printing of pillars. Using the CAD file, any design scheme can be implemented on the glass unit and the desired pillar thickness can be achieved by multi-pass printing. This approach shows promise for addressing the challenges associated with the pillar placement and reliability associated with the current pick-n-place approach. We also printed a vacuum valve using the additive manufacturing technique. A laser powder bed Form Up 350 system was used to print the valve using maraging steel that offers the optimum balance of material weight and strength for demanding engineering applications. As shown in Figure 15, complex 3D valve geometries can be easily manufactured using additive manufacturing techniques at a feature size control well below 100 μm.

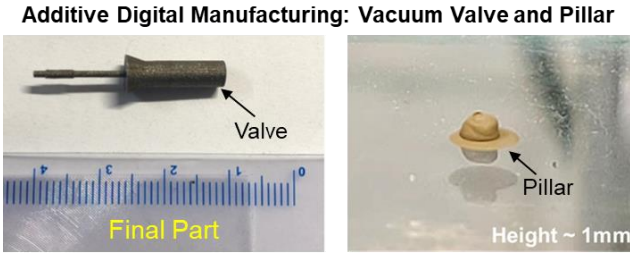

Figure 15 *Additive manufacturing and integration of VIG components.*

Fabrication of VIG Prototype:

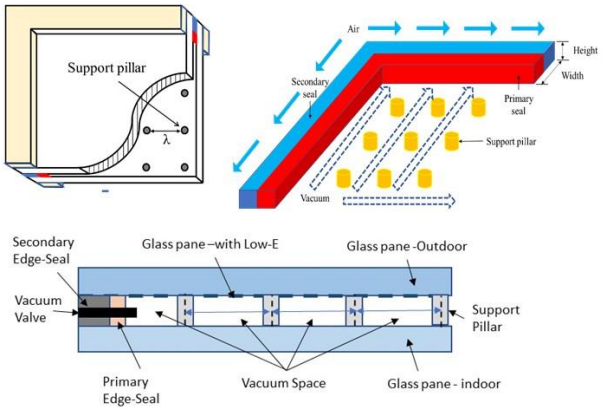

Figure 16 *Construction details of the VIG prototype.*

Based on our analytical analysis and experimental results, the team prepared a VIG prototype 20 in. long by 14 in. wide. This prototype (see Figure 16) used 3 mm low-E glass from Cardinal with an emissivity of 0.018 and 3 mm clear glass from Vitro with a vacuum space 1 mm high. Pillars made from proprietary ceramic material of 1 mm were used and were spaced 50 mm apart in a gridded pattern. A proprietary flexible seal with separate formulation was used as the primary and secondary edge seal. The primary edge seal width was 5 mm, and the secondary seal width was 7.5 mm. Our state-of-the-art vacuum valve is successfully integrated into the VIG from the side by inserting it between the two glazing and sealing it along with the primary and secondary seal. The side insertion helped us to reduce surface stresses, obtain evenly spaced out pillars, and ease fabrication. In conventional VIG manufacturing, the valve is inserted by drilling a hole in one of the glass panes, which induces stresses and makes the fabrication process complex. This also allows us to evenly space the pillars in the VIG compared with pillar placement in the conventional VIG, which has more pillars concentrated near the vacuum valve.

We used a conventional direct drive rotary vane vacuum pump with booster to draw vacuum from our prototype, see Figure 17. We were able to achieve the desired vacuum of 10^{-3} Torr, which would result in a VIG R-Value of R-9, including the edge seal effect.

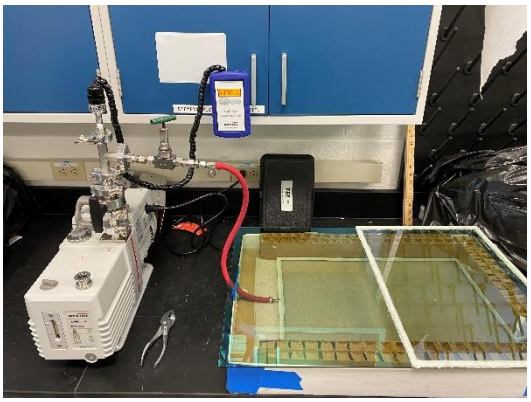

Figure 17 *VIG prototype and conventional direct drive rotary vane vacuum pump*

Highlight features of our prototype VIG sample:

- ✓ VIG has a flexible seal with an elastic modulus (*E*) of 3.78 MPa, which is flexible enough to resist the stress induced by temperature gradients in the VIG.
- ✓ A state-of-the-art vacuum valve is successfully integrated into the VIG from the side by inserting it between the two glazing panes.
- ✓ Our edge seal does not require any oven or laser curing. Oven and laser curing requires specialized machines, human safety, and skills that result in high overhead costs.
- ✓ Our nonmetallic pillars are evenly placed in the VIG; therefore, the placement can be easily automated. The pillars are made of proprietary material with low thermal conductivity and that resists all induces stresses.
- ✓ Our VIG can be evacuated using a conventional rotary vane pump to achieve 10^{-3} Torr.
- ✓ Induced stresses in our VIG design are very low compared with other conventional VIGs and therefore might not require tampered glazing.

Our VIG is very cost effective and can be introduced in the market at a cost comparable with current high-performance dual insulated glass units.

Conclusion

A scalable, low-cost processing strategy for glass strengthening and sealing of VIG units has been explored and developed during this project. The sealing and pillar design were optimized based on FEA modeling and calculation, and the glass panes were strengthened by scalable PAL photonic processing. Various laser sealing parameters including sample traveling speed, spot diameter, and laser power were optimized through response surface methodology and showed the effectiveness of laser processing compared with the thermally cured method. Components of the VIG units, the vacuum valve and pillars, were successfully produced by additive manufacturing, and a VIG prototype of 20 in. long by 14 in. wide was successfully fabricated. We were able to achieve the desired vacuum of 10^{-3} Torr, which would result in the VIG R-Value of R-9, including the edge seal. The prototype VIG sample has several unique features and is very cost effective compared with current high-performance dual-insulated glass units.

Future R&D Focus Areas and Next Steps

- After successful integration of our state-of-the-art vacuum valve in our prototype VIG, as a next step, develop automated spot welding of multiple vacuum valves after the vacuum has been created in a line of multiple VIGs to meet industrial production process requirements.
- Perform thermal conductivity tests, both ISO-19916 and ASTM C518, to verify the performance. Also, test the edge of the glazing area to determine the overall performance of the VIG unit, that is, center-of-glass and edge-of-glass conductivity.
- Perform ASTM E 2190 durability testing on our prototype, which is 20 in. long by 14 in. wide. Also test a larger prototype, which will be 40 × 20 in., to verify resistance to linear stress failure.
- Prepare a real-sized fixed window with VIG installed in the window and test the unit to all required ASTM and industry thermal and structural standards.
- Work with industrial partners to deploy the developed VIG unit in the market.
- Develop a special coating that can be applied to the outside surface of the glazing to help resist breakage from induced field stresses and to avoid outdoor condensation.
- Develop more economical means to heat strengthen the glass using nanotechnology.

Acknowledgments

This work is supported by the Buildings Technology Office of the US Department of Energy, and we specifically thank Marc LaFrance at the US Department of Energy for guiding this research.

Innovation and Patent

US Nonprovisional Patent Application
Title: Vacuum Insulation Glazing, Valve, Flexible Seal, and Method for Making Vacuum Insulated Glazing
ID 4214.1; Appl. No.: 17/570,931

Publications

1. Zhu, W., Zhang, S., Shin, S., Gorti, S., Shah, B., Joshi, P., and Bhandari, M. 2022. "Effects of pillar design on the thermal performance of vacuum-insulated glazing." *Construction and Building Materials* 316: 125724.
2. Zhang, L., Zhang, S., Joshi, P., Bhandari, M., Hu, A., and Shin, S. 2022. "Laser strengthening of additive manufactured edge seal for vacuum insulated glazing with micro-size glass frit." *Journal of Building Engineering* 53: 104539.
3. Zhu, W., Shah B., Gorti, S., Bhandari, M., Sabau, A., and Shin, S. "Effects of Edge-Seal Design on the Mechanical and Thermal Performance of Vacuum-Insulated Glazing." (Submitted to: *Building and Environment*).

References

1. Review of Cost Effectiveness Analysis. ENERGY STAR for Windows, Doors, and Skylights Version 6.0 Criteria Revision.
2. Benson, D. K., et al. 1990. Vacuum window glazings for energy-efficient buildings (No. SERI/TP-212-3684). Solar Energy Research Inst., Golden, CO (USA).
3. Ng, N., R. E. Collins, and L. So. 2007. "Characterization of the thermal insulating properties of vacuum glazing." *Materials Science and Engineering: B* 138(2): 128–134.
4. Lux, C., B. Nusser, and P. Schober. 2020. "Experimental investigations on airborne sound insulation of vacuum insulating glazing (VIG)." I*NTER-NOISE and NOISE-CON Congress and Conference Proceedings.* Vol. 261. No. 5. Institute of Noise Control Engineering.
5. Memon, S. 2013. Design, fabrication and performance analysis of vacuum glazing units fabricated with low and high temperature hermetic glass edge sealing materials. Loughborough University.
6. Martins, J., et al. 2020. "Novel laser-assisted glass frit encapsulation for long-lifetime perovskite solar cells." *Journal of Materials Chemistry A* 8(38): 20037–20046.
7. Cuce, E., and P. M. Cuce. 2016. "Vacuum glazing for highly insulating windows: Recent developments and future prospects." *Renewable and Sustainable Energy Reviews* 54: 1345–1357.
8. ABAQUS 3DEXPERIENCE R2017x, 2017. Dassault Systemes SIMULIA Corp., Johnston, RI.